

Accuracy and Integrity Potential of Multichain Navigation

Jaime Cruz and Robert Stoeckly
Illgen Simulation Technologies, Inc.
jcruz@illgen.com, rstoeckly@illgen.com

ABSTRACT

This paper describes autonomous integrity monitoring algorithms that can be used for validating the measurements, error models, functional model, and measurement geometry used in an all-in-view Loran navigation. The algorithms consist of the chi-square test, t-test, and reliability metrics calculations. The chi-square test is applied for overall “goodness-of-fit” assessment of the adjustment system. The t-test is applied for outlier detection and exclusion in the individual measurements. Reliability metrics are applied for assessing the strength of observing geometry with respect to blunder detection. The internal reliability measure is the maximum undetectable gross error in the observations, given designed probabilities of missed detection and false detection. The external reliability measure is the position shift due to the maximum undetectable error. Whenever the external reliability metric exceeds the alarm limit for the phase of flight, the integrity monitoring function is considered unavailable. A novel feature of the accuracy and integrity computations presented is the use of a full covariance matrix of the a priori ASF/ED errors in the observation weighting and error propagation. The ASF/ED error covariance model is discussed in a companion paper.

1. Introduction

Illgen Simulation Technologies, Inc. (ISTI) is developing a weighted GPS/Loran-C position model and is leading an activity to develop a steerable H-field antenna to work with the all-in-view Loran receiver. The goal of the program is to show that the Loran-C component of a hybrid GPS/Loran system can meet the requirements for horizontal navigation and approach procedures during loss of the GPS signal. The results of the effort on the all-in-view Loran navigation algorithm development are reported in [1].

Figure 1 presents a simplified schematic of the algorithm system proposed in [1]. There are ten numbered algorithm blocks shown. The development in [1] focused on the analysis, prototyping, and testing of Blocks 2 (Interchain Phase Ambiguity Resolution), 3 (Closed-form triad solution), 5 (A priori ASF/ED Error Model), 7 (ASF/ED Prediction), 8 (TOA Error Model), and 10 (Least Squares Navigation with OTF ASF Calibration and RAIM). The paper [2] presents the developments related to the modeling of a priori ASF/ED errors and their treatment in the navigation estimation (Blocks 5, 7, and part of 10). This paper presents the results to date of the development of the Receiver Autonomous Integrity Monitoring (RAIM) component of Block 10. As the project progresses it is hoped that a future paper will present the results of an end-to-end implementation, real data testing, and tuning of the system shown in Figure 1.

This paper is organized as follows. Section 2 gives the least squares equations used in the navigation. Section 3 discusses the observation error model. Section 4 gives the chi-square test used for overall assessment of the adjustment system. Section 5 describes the t-test used for blunder detection and exclusion. Sections 6 and 7 discuss the reliability measures used to assess the availability of safety of navigation. Section 8 discusses the verification and validation tests performed on the accuracy and proposed RAIM equations. Finally, Section 9 gives the summary and recommendations.

2. Least Squares Estimation Equations

Start with the non-linear observation model:

$$(2-1) \quad L_a = F(X_a)$$

where:

F ... Known vector function
 L_a ... Theoretical observation vector
 X_a ... True value of the parameter vector to be estimated.

The linearized observation equation becomes:

$$(2-2) \quad L_b + V_a = F(X_0) + A(X_a - X_0)$$

$$(2-3) \quad A \equiv \left. \frac{\partial F}{\partial X_a} \right|_{X_a=X_0}$$

where:

L_b ... Observation (measurement) vector
 V_a ... Theoretical residual vector, arising from measurement and modeling errors
 X_0 ... Linearization point
 A ... Representation of the geometry of the Loran-C transmitters, called the design matrix.

The linearized observation equation can be re-written as:

$$(2-4) \quad V_a = AX - L$$

$$(2-5) \quad X \equiv X_a - X_0$$

$$(2-6) \quad L \equiv L_b - F(X_0).$$

We have the null hypothesis:

$$(2-7) \quad H_0 : L \rightarrow N(AX, \sigma_0^2 W^{-1}).$$

That is, the (observed – computed) vector has a multi-dimensional Normal distribution with expectation AX and dispersion $\sigma_0^2 W^{-1}$, where:

W ... Weight matrix of the observations
 σ_0 ... A priori reference standard deviation (usually set to 1)

The least squares minimization principle is:

$$(2-8) \quad V^T W V \rightarrow \text{minimum}$$

where V is the post-estimation residual vector. This leads to the parameter estimate:

$$(2-9) \quad \hat{X} = (A^T W A)^{-1} A^T W L.$$

The residuals of the adjustment are:

$$(2-10) \quad V = A \hat{X} - L.$$

Under the null hypothesis, the probability distributions of \hat{X} and V are:

$$(2-11) \quad \hat{X} \rightarrow N(X, \sigma_0^2 Q_{XX})$$

$$(2-12) \quad V \rightarrow N(0, \sigma_0^2 Q_{VV})$$

with the co-factor matrices:

$$(2-13) \quad Q_{XX} = (A^T W A)^{-1}$$

$$(2-14) \quad Q_{VV} = W^{-1} - A Q_{XX} A^T.$$

An a posteriori estimate of the reference variance can be computed from the weighted sum of squared residuals and the number of degrees of freedom:

$$(2-15) \quad \hat{\sigma}_0^2 = \frac{V^T W V}{r}$$

$$(2-16) \quad r \equiv n - u$$

where:

n ... Number of observations
 u ... Number of unknown parameters being estimated
 r ... Number of degrees of freedom of the adjustment.

3. Observation Error Model

The error covariance matrix of the (observed – computed) residuals (2-6), equal to the inverse of the weight matrix assuming $\sigma_0^2 = 1$, is expressed as:

$$(3-1) \quad W^{-1} = W_1^{-1} + W_2^{-1}$$

where:

W_1^{-1} ... Error covariance matrix of the TOA measurements
 W_2^{-1} ... Error covariance matrix of the ASFs.

The error covariance matrix of the ASFs is computed using the model described in [2] Sections 3 and 4. The model is based on double path integration of a postulated homogeneous and isotropic covariance function of scale factor errors, where the scale factor is defined to be the reciprocal of the phase velocity. The scale factor error covariance function used in the tests has a variance of 0.108 m/km and correlation length of 200 km. Deviations from this nominal case are explicitly stated in the discussion of test results.

The error covariance matrix of the TOA measurements is expressed as:

$$(3-2) \quad W_1^{-1} = \begin{bmatrix} \sigma_1^2 & \sigma_{1,2} & \cdots & \sigma_{1,n} \\ \sigma_{1,2} & \sigma_2^2 & \cdots & \sigma_{2,n} \\ \vdots & \vdots & \ddots & \vdots \\ \sigma_{1,n} & \sigma_{2,n} & \cdots & \sigma_n^2 \end{bmatrix}$$

where n is the number of observations, and:

$$(3-3) \quad \sigma_i^2 = \sigma_{i,noise}^2 + \sigma_{sta_clk}^2 + \sigma_{chain_clk}^2 + \sigma_{other}^2$$

$$(3-4) \quad \sigma_{i,noise} = \frac{50}{SNR_i} \text{ (meters); SNR is the}$$

unitless signal-to-noise amplitude ratio as measured by the receiver

$$(3-5) \quad \sigma_{sta_clk} = 10 \text{ m (Standard deviation of Loran-C clock synchronization error among station clocks within the same chain)}$$

$$(3-6) \quad \sigma_{chain_clk} = 30 \text{ m (Standard deviation of Loran-C clock synchronization error among master clocks of the different chains)}$$

$$(3-7) \quad \sigma_{other} = 40 \text{ m.}$$

The off-diagonal elements in (3-2) are:

$$(3-8) \quad \sigma_{i,j} (i \neq j) = \begin{cases} 0, & \text{if stations } i \text{ and } j \text{ do not} \\ & \text{belong to the same chain} \\ \sigma_{chain_clk}^2, & \text{if stations } i \text{ and } j \text{ belong} \\ & \text{to the same chain.} \end{cases}$$

The error (3-5) arises because the service area monitor (SAM) does not respond immediately when the measured time difference (TD) drifts from the controlling standard time difference (CSTD). The errors (3-6) and (3-8) arise from the mis-synchronization of the master clocks relative to UTC. The error (3-7) covers unmodeled error sources such as carrier-wave interference not removed by notch filters, cross-rate interference not removed by the receiver, and skywave contamination not removed by the receiver.

4. Statistical Test on the A Posteriori Reference Variance

A statistical test on the a posteriori reference variance may be used to assess the overall “goodness-of-fit” of the adjustment system. If the

test fails, possible causes include (a) measurement blunders, (b) deficiency in the measurement error model, and (c) deficiency in the functional model relating observations and parameters.

We compute the test statistic:

$$(4-1) \quad \chi_r^2 = \frac{r\hat{\sigma}_0^2}{\sigma_0^2}.$$

This statistic has a χ^2 (chi-square) distribution with r degrees of freedom, where r = redundancy in the adjustment.

The two-sided test has the following null and alternative hypotheses:

$$(4-2) \quad \begin{aligned} H_0 : \sigma^2 &= \sigma_0^2 \\ H_1 : \sigma^2 &\neq \sigma_0^2 \end{aligned}$$

H_0 is rejected if:

$$(4-3) \quad \chi_r^2 < \chi_{1-\alpha/2,r}^2 \text{ or } \chi_r^2 > \chi_{\alpha/2,r}^2$$

since

$$(4-4) \quad P\{\chi_{1-\alpha/2,r}^2 < \chi_r^2 < \chi_{\alpha/2,r}^2\} = 1 - \alpha$$

where α is the significance level of the test and $P\{\cdot\}$ is the probability operator. When the functional and stochastic modeling is mature, it is usual to apply only the one-sided upper-bound test for the purpose of fault detection. Table 1 gives the upper and lower chi-square thresholds needed in (4-3) for various degrees of freedom and two-tail test significance level of $\alpha = 0.01$.

5. Student t Test for Blunder Detection and Exclusion

While the chi-square test provides an overall fault detection, the t-test provides specific fault detection and exclusion with regards to individual measurements. The null and alternative hypotheses are:

$$(5-1) \quad \begin{aligned} H_0 : E(v_i) &= 0 \\ H_1 : E(v_i) &\neq 0 \end{aligned}$$

where v_i is the i -th residual and $E(\cdot)$ is the expectation operator.

The test statistic is computed as:

$$(5-2) \quad t_i = \frac{|v_i|}{\sigma_0 \sqrt{q_{v_i v_i}}}$$

where $q_{v_i v_i}$ is the i -th diagonal element of the Q_{VV} matrix.

H_0 is rejected if:

$$(5-3) \quad t_i > t_{\alpha, r}$$

since

$$(5-4) \quad P\{t_i < t_{\alpha, r}\} = 1 - \alpha$$

where α is the significance level of the test and r is the redundancy in the adjustment. Table 2 gives the t-test threshold needed in (5-3) for various degrees of freedom and test significance level of $\alpha=0.001$.

6. Internal Reliability Measure

The chi-square and t tests form only part of the assessment of the adjustment system. Portions of measurement errors that do not cause adjustment residuals remain undetected by the chi-square and t tests. Therefore the internal reliability of the system, defined as the ability of the measurement geometry to detect blunders, should also be assessed to the required probability level. The ability to detect blunders depends directly on the redundancy of the measurement geometry.

The effect of an error vector ∇L on the adjusted residuals is found using (2-9), (2-10), and (2-14):

$$(6-1) \quad \nabla V = [A(A^T W A)^{-1} A^T W - I] \nabla L$$

or,

$$(6-2) \quad \nabla V = -(Q_{VV} W) \nabla L.$$

The matrix $Q_{VV} W$ (call it the M matrix) may be referred to as a redundancy matrix and has the following characteristics:

- M is an idempotent matrix ($MM = M$), and so trace (M) = rank (M).
- From (6-1), trace (M) = n-u = redundancy of the system.

- The diagonal elements of M , denoted by r_i , have values between 0 and 1 ($0 \leq r_i \leq 1$).

The effect of the i -th error ∇l_i on the i -th residual is expressed as:

$$(6-3) \quad \nabla v_i = r_i \nabla l_i$$

where r_i is the i -th diagonal element of the $Q_{VV} W$ matrix, and is called the redundancy number of the i -th observation. The smaller the redundancy number, the smaller the effect of the measurement error on the corresponding residual. The ideal geometry spreads the total redundancy (n-u) evenly among the n measurements.

For the internal reliability measure, we use the formulations from [3] and [4]. The measure, denoted as $\nabla_0 l_i$, is the maximum undetectable gross error in an observation for designed probabilities of missed detection and false detection. The measure can be derived from (6-3):

$$(6-4) \quad \nabla_0 l_i = \frac{\delta \sigma_0 \sqrt{q_{v_i v_i}}}{r_i}$$

where δ is the non-centrality parameter, which is the sum of the multipliers K_{fa} and K_{md} for achieving the required probability of false alarm (P_{fa}) and probability of missed detection (P_{md}) in the fault detection test (5-1). See Figure 2. The numerator in (6-4) is the maximum undetectable error in the residual for the given probabilities.

7. External Reliability Measure

The external reliability of the adjustment system measures the effect of the maximum undetectable gross error (6-4) on the estimated parameters. Using (2-9), this effect is:

$$(7-1) \quad \nabla_0 \hat{X}_i = S_i \nabla_0 l_i$$

where S_i is the i -th column of the projection matrix defined as:

$$(7-2) \quad S = (A^T W A)^{-1} A^T W.$$

For the external reliability measure, we use the position shift component of (7-1). Assuming the vector elements are ordered as (East, North, Time bias), the position shift due to the maximum

undetectable error in the i -th observation is computed as the RSS of the first and second elements of the vector from (7-1):

$$(7-3) \quad \nabla_0 p_i = \sqrt{(\nabla_0 \hat{x}_{i1})^2 + (\nabla_0 \hat{x}_{i2})^2}.$$

8. Accuracy and RAIM tests

This section describes the verification and validation tests performed to assess the accuracy and integrity equations given in the previous sections. The tests are limited to the use of a test data set in the Madison, WI area. For sensitivity analysis, results using two versus five chains, and different assumptions on the variance and correlation length of the scale factor error are compared.

8.1 Implementation Notes

The test data set was received from Locus, Inc. in connection with an earlier task. The data set was gathered by a Locus LRS receiver on June 24, 1994 in the late afternoon. In the data set the receiver is being driven around a loop of size roughly 2.5 nautical miles in longitude and 5 nautical miles in latitude in the Madison, Wisconsin area. The file gives data nominally every 15 seconds, starting at a time tag of 360 and ending at 1950 seconds.

The two-chain test case involved GRIs 8970 (Great Lakes) and 9960 (Northeast U.S.). The five-chain case involved additionally GRIs 8290 (North Central U.S.), 9610 (South Central U.S.), and 7980 (Southeast U.S.).

The test software implemented Block 10 of Figure 1. The inputs consisted of (a) observation residuals and partial derivatives as computed using the Loran-C positioning software received from Locus, Inc. in October 1999 and (b) observation error model from (3-1). The ASF model used in the Locus program to form the observation residuals was based on a uniform regional conductivity of 0.005 S/m. The atmospheric index of refraction used had a value of 1.000338 at the Earth's surface and a vertical lapse rate of $(1-\alpha)/R$, where $\alpha = 0.75$ and R is the radius of the Earth. No external position or time updates were used, i.e., the tests corresponded to stand-alone Loran. As indicated in [2] Equation (2-22), the on the fly ASF calibration aspect of these tests relates to the use of the formal uncertainties of the a priori ASFs in the observation weighting. This is equivalent to

using receiver-only errors in the weighting but adjusting the ASFs along with the navigation estimation.

8.2 Numerical Results

Figures 3 and 4 plot, for the five-chain and two-chain cases respectively, the time history of the minimum and maximum observation sigmas (standard errors) as computed from (3-1). The figures show both TOA-only and TOA/ASF contributions. The observation TOA-only sigmas range from 40 to 400 m for the five-chain case, and 40 to 180 m for the two-chain case. The observation TOA/ASF sigmas range from 60 to 420 m for the five-chain case, and 60 to 220 m for the two-chain case.

Figure 5 plots time history of the 2DRSS position error and lengths of the semimajor and semiminor axes of the error ellipse, before fault detection and exclusion via the t-test. The computation is based on the error covariance matrix (2-13). The 2DRSS is defined as twice the square-root of the sum of the squares of the east and north standard errors. The (2DRSS, semimajor, semiminor) values are typically (120, 50, 30) meters, except for a roughly 300-sec period of poor SNRs when the values reach (180, 80, 40) meters.

Figure 6 is the same as Figure 5 except that the results reflect the t-test detection and exclusion of measurement outliers at the 0.001 significance level. For example, at time tag 481 seconds the t-test excluded eight out of 20 measurements. The excluded measurements otherwise appeared acceptable based on the flags provided by the receiver. Four of the excluded measurements had obviously large residuals of 2.5 to 3 km compared to the nominal residuals of 50 to 200 m. The other four excluded measurements had marginally high residuals of 220 to 400 m. The t-test results were encouraging because two of the large outliers (8970W Malone, FL and 7980X Raymondville, TX) were flagged as bad by the receiver itself on the very next epoch. The receiver also flagged the other two large outliers (9610X Las Cruces, NM and 9610Y Raymondville, TX) after one more epoch.

Figure 6 shows the 2DRSS increasing to 270 m at epoch 1185 seconds because the t-test deleted 12 out of 20 measurements. The problem appeared real since the receiver itself flagged 10 of the 20 measurements at the very next epoch. At the next two epochs (1200 and 1215) the t-test did not find

at least four good measurements out of the 10 and 11 unflagged ones and so there is no solution shown in Figure 6. For the rest of the time period the t-test deleted only one to three measurements, which were clearly outliers related to 8290M Havre, MT and 9610Z Grangeville, LA, except at epoch 1950 where five outliers were deleted. Overall, the t-test achieved good performance in these tests.

Figure 7 shows the time history of the two-tail, 0.01 significance level, chi-square test results after outlier deletions by the t-test. The chi-square test is valuable during system tuning of the observation error model. The figure indicates a reasonably well-tuned model since most of the cases are within bounds. More tests are needed. From the safety point of view it is more important to focus on the cases when the chi-square statistic is greater than the upper bound than when it is less than the lower bound. After system tuning the chi-square test may be used in addition to the t-test in order to reject the navigation solution when the test fails at an epoch.

Figure 8 compares the time history of the 2DRSS position error for the two-chain and five-chain cases. The t-test has been applied in both cases. The two results are not very different, with a nominal 2DRSS of 120 m for the five-chain case and 140 m for the two-chain case. This indicates rather weak sensitivity of accuracy to the number of TOA measurements (9 versus 21).

Figure 9 compares the time history of the position shift caused by the maximum undetectable blunder for the two-chain and five-chain cases. The position shift was computed as the maximum value of (7-3) over all measurements at each epoch. The assumed probabilities were 10^{-3} for missed detection and 10^{-6} for false alarm (Figure 2). It is seen that there is a dramatic increase in the availability of integrity (safety) in going from two to five chains. The five-chain geometry provides a horizontal bound (protection level) of about 320 m, whereas the two-chain geometry provides a bound of about 1450 m.

Figure 10 shows the sensitivity of the 2DRSS position error to the parameters of the scale factor error covariance function. There is little sensitivity in going from the nominal correlation length of 200 km (as used in all the above tests) to 500 km. However, when the scale factor standard error is doubled to 0.216 m/km the 2DRSS error increased from 120 to 210 m. At epoch 1200 seconds, when

the t-test did not find at least four good measurements in the nominal case, the increased scale factor error variance caused four measurements to be accepted; so, the resulting 2DRSS reached 570 m.

Figure 11 shows the sensitivity of the availability of integrity to the parameters of the scale factor error covariance function. The horizontal protection level increases from 310 to 440 m when the scale factor error correlation length increases from 200 to 500 km. The protection level increases dramatically to 1400 m when the scale factor standard error is doubled to 0.216 m/km. Whenever the protection level exceeds the alarm limit for the phase of flight, the integrity monitoring function is considered unavailable. Therefore, it appears that the ASF/ED-related errors can drive the availability of the integrity monitoring function. This emphasizes the importance of calibrating the ASF/ED errors using for example the techniques discussed in [2].

9. Summary and Recommendations

This paper presents autonomous integrity monitoring algorithms for all-in-view Loran navigation and shows some encouraging results. As a general recommendation, the algorithms developed in this paper should be implemented in an end-to-end system as described in [1] and shown in Figure 1. The system should be tested and tuned with real data, all-in-view receiver, and truth navigation using GPS. The following specific recommendations are made.

During system testing and tuning, it is recommended that the chi-square test (Section 4) be applied for overall assessment of the “goodness-of-fit” of the adjustment system. Specifically, this will help calibrate the measurement and ASF/ED error model parameters.

During system testing and tuning, it is recommended to continue validating the performance of the t-test (Section 5) with regards to reliable fault detection and exclusion in individual TOA measurements.

During system testing and tuning, it is recommended to continue validating the performance of the reliability metrics (Sections 6 and 7) with regards to assessing the availability of integrity of Loran-C navigation.

REFERENCES

[1] “Loran-C Augmentation for GPS and GPS/WAAS, Volume 1: All-In-View Algorithm Development”, Illgen Simulation Technologies, Inc., IST2000-R-242, October 2000.
 [2] “Covariance Analysis for On-the-fly ASF Calibration During Multichain Navigation”, J. Cruz, Illgen Simulation Technologies, Inc., presented at the International Loran Association 29th Annual Convention and Technical Symposium, November 2000.
 [3] “A Testing Procedure for Use in Geodetic Networks”, W. Baarda, Netherlands Geodetic Commission, Publications on Geodesy, Volume 2, Number 4, Delft 1967.
 [4] “The Accuracy Potential of the Modern Bundle Block Adjustment in Aerial Photogrammetry”, A. Grün, Photogrammetric Engineering and Remote Sensing, Vol. 48, No. 1, pp. 45-54, January 1982.

BIOGRAPHIES

Jaime Cruz is a Principal Engineer with the Navigation and Communications Division at ISTI. He has worked for five years on navigation with the Global Positioning System and the FAA’s Wide Area Augmentation System. His previous

experience included local and global gravity field modeling for ICBM targeting, positioning of ground targets using a satellite-borne laser ranging system, satellite orbit estimation, and development of an airborne gravity measuring system for oil exploration. Dr. Cruz received his MS (1982) and Ph.D. (1985) in geodesy from The Ohio State University.

Robert Stoeckly has worked in radionavigation since 1997 as Senior Research Engineer at ISTI. His research includes experimental and theoretical work in Loran-C and simulations of the Wide Area Augmentation System. Dr. Stoeckly previously developed physics models for the simulations of atmospheric nuclear bursts and their effects on the performance of communications systems. He received the Ph.D. in astrophysical sciences from Princeton University in 1964.

ACKNOWLEDGEMENT

The work described in this paper was sponsored by the “FAA AND-740 Loran-C Augmentation for GPS and GPS/WAAS” Program under Grant 99-G-038.

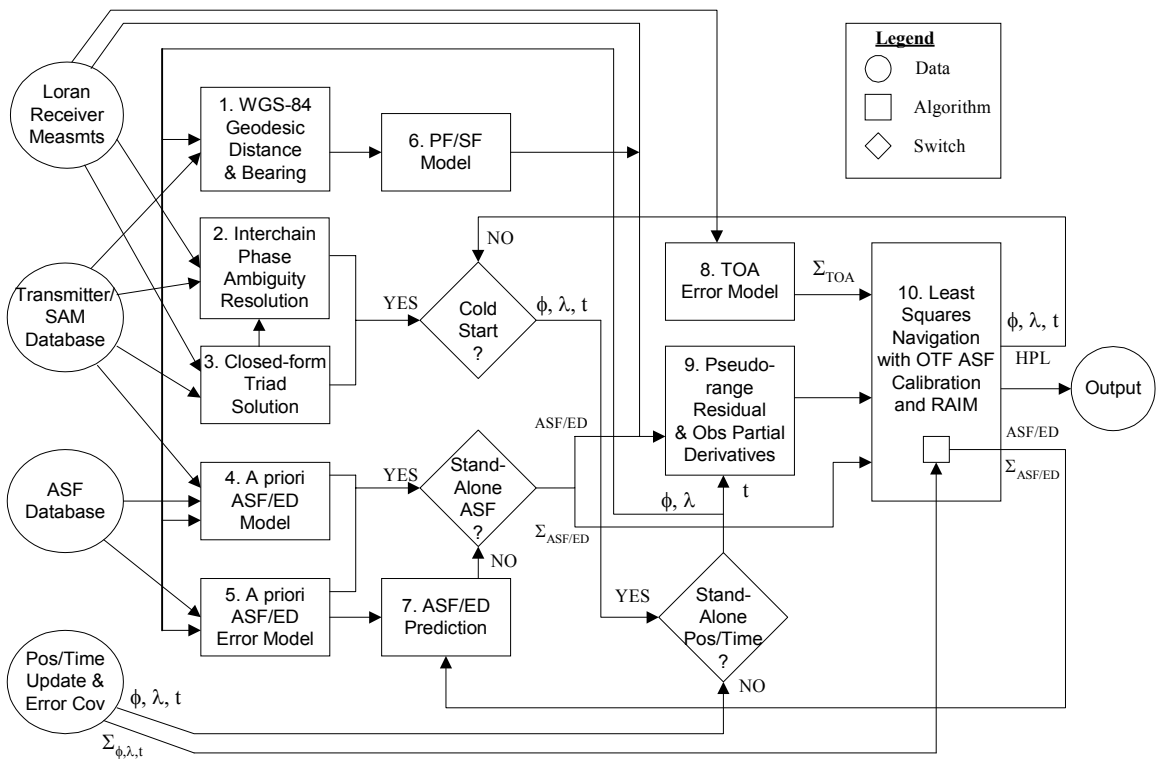


Figure 1. Simplified schematic of all-in-view Loran navigation algorithms.

Table 1. Upper and lower chi-square test thresholds, for given degrees of freedom r and two-tail test significance level $\alpha = 0.01$. Optionally, one can apply the upper threshold only in a one-sided upper-bound test with significance level of 0.005.

Degrees of Freedom r	Lower Threshold $\chi^2_{1-\alpha/2,r}$	Upper Threshold $\chi^2_{\alpha/2,r}$	Degrees of Freedom r	Lower Threshold $\chi^2_{1-\alpha/2,r}$	Upper Threshold $\chi^2_{\alpha/2,r}$
1	0.00	7.88	16	5.14	34.27
2	0.01	10.60	17	5.70	35.72
3	0.07	12.84	18	6.26	37.16
4	0.21	14.86	19	6.84	38.58
5	0.41	16.75	20	7.43	40.00
6	0.68	18.55	21	8.03	41.40
7	0.99	20.28	22	8.64	42.80
8	1.34	21.96	23	9.26	44.18
9	1.73	23.59	24	9.89	45.56
10	2.16	25.19	25	10.52	46.93
11	2.60	26.76	26	11.16	49.29
12	3.07	28.30	27	11.81	49.64
13	3.57	29.82	28	12.46	50.99
14	4.07	31.32	29	13.12	52.34
15	4.60	32.80	30	13.79	53.67

Table 2. t-test threshold $t_{\alpha,r}$ for given degrees of freedom r and test significance level $\alpha = 0.001$.

Degrees of Freedom r	Threshold $t_{\alpha,r}$	Degrees of Freedom r	Threshold $t_{\alpha,r}$	Degrees of Freedom r	Threshold $t_{\alpha,r}$
1	636.619	11	4.437	21	3.819
2	31.598	12	4.318	22	3.792
3	12.941	13	4.221	23	3.762
4	8.610	14	4.140	24	3.745
5	6.859	15	4.073	25	3.725
6	5.959	16	4.015	26	3.707
7	5.405	17	3.965	27	3.690
8	5.041	18	3.922	28	3.674
9	4.781	19	3.883	29	3.659
10	4.587	20	3.850	30	3.646

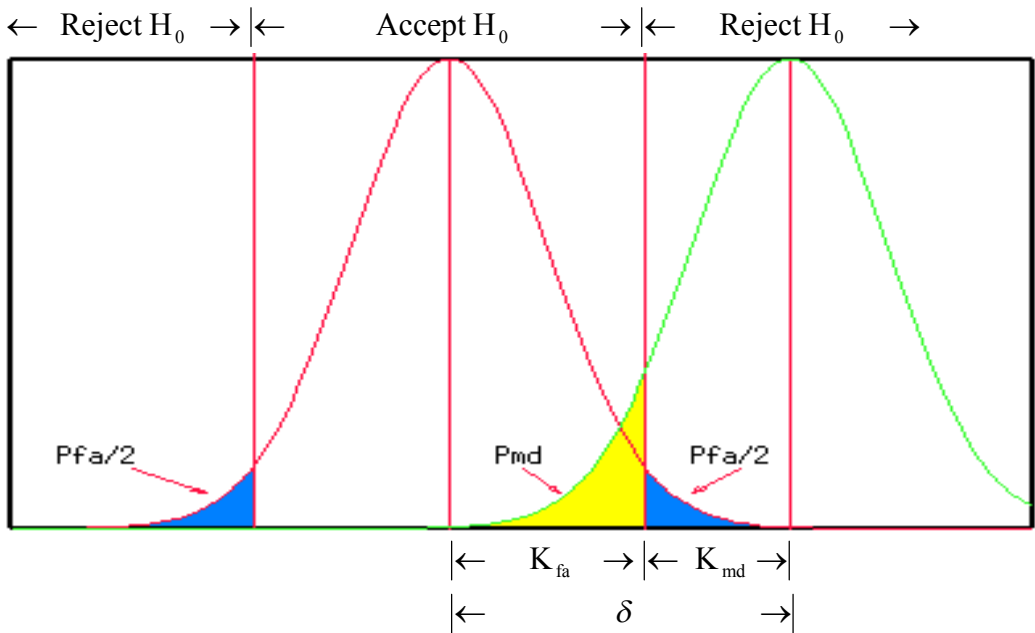


Figure 2. Non-centrality parameter δ for satisfying designed probabilities of missed detection (P_{md}) and false alarm (P_{fa}). The K_{fa} and K_{md} are multipliers of the standard deviation (assumed unity in the figure) to achieve the required one-tail probability P_{md} and two-tail probability P_{fa} for a Normal distribution. For example, $P_{fa} = 10^{-6}$ and $P_{md} = 10^{-3}$ give $K_{fa} = 4.89$, $K_{md} = 3.09$, and $\delta = 7.98$.

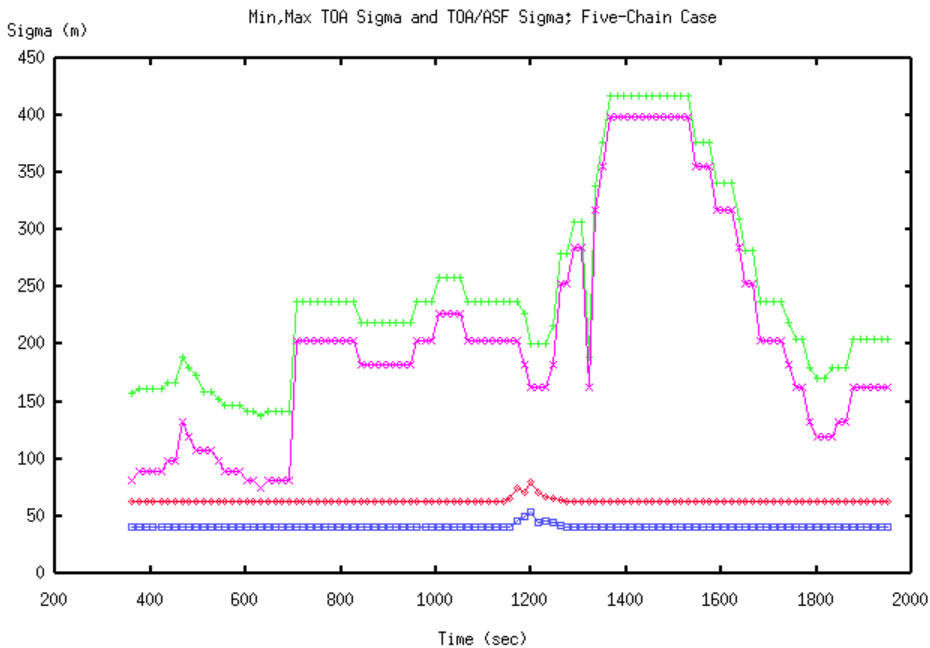


Figure 3. Minimum and maximum standard error of the observations for the five-chain case. The lowest and third lowest curves account for receiver errors only, while the remaining two curves account for both receiver and ASF/ED modeling errors.

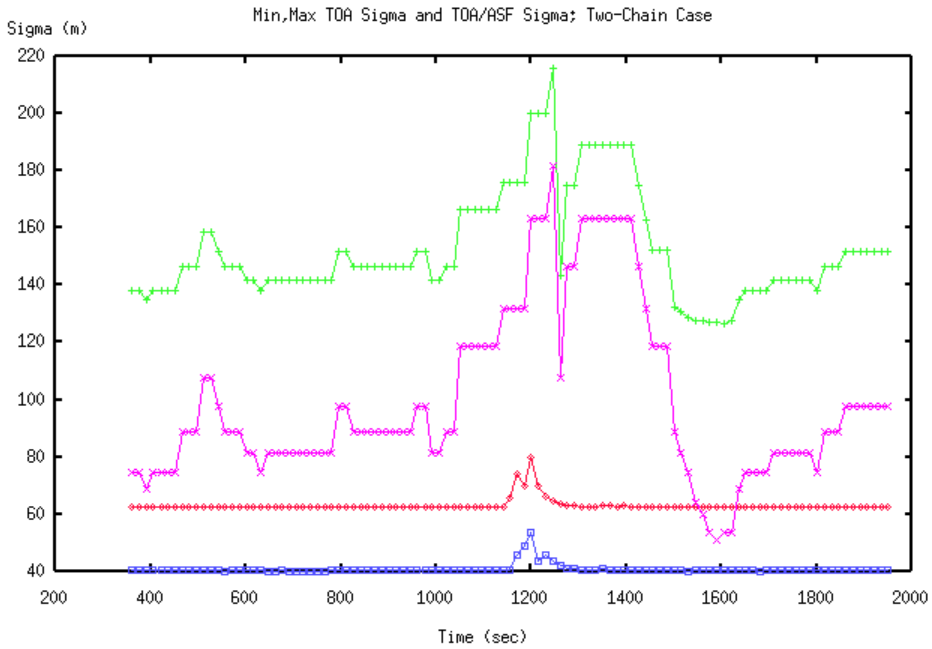


Figure 4. Minimum and maximum standard error of the observations for the two-chain case. The lowest and third lowest curves account for receiver errors only, while the remaining two curves account for both receiver and ASF/ED modeling errors.

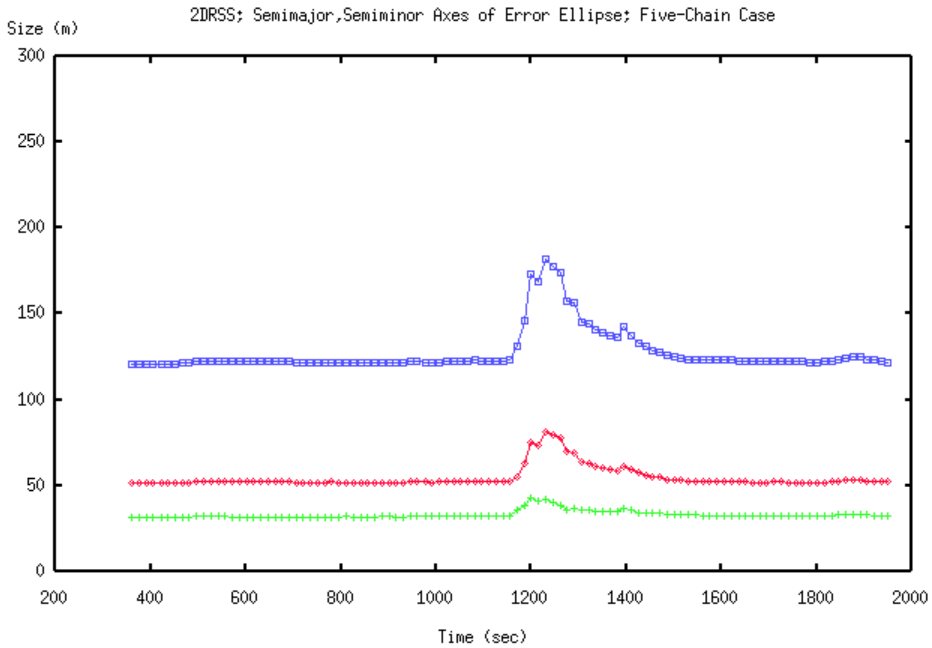


Figure 5. 2DRSS position error and lengths of the semimajor and semiminor axes of the error ellipse for the five-chain case before fault detection and exclusion via the t-test.

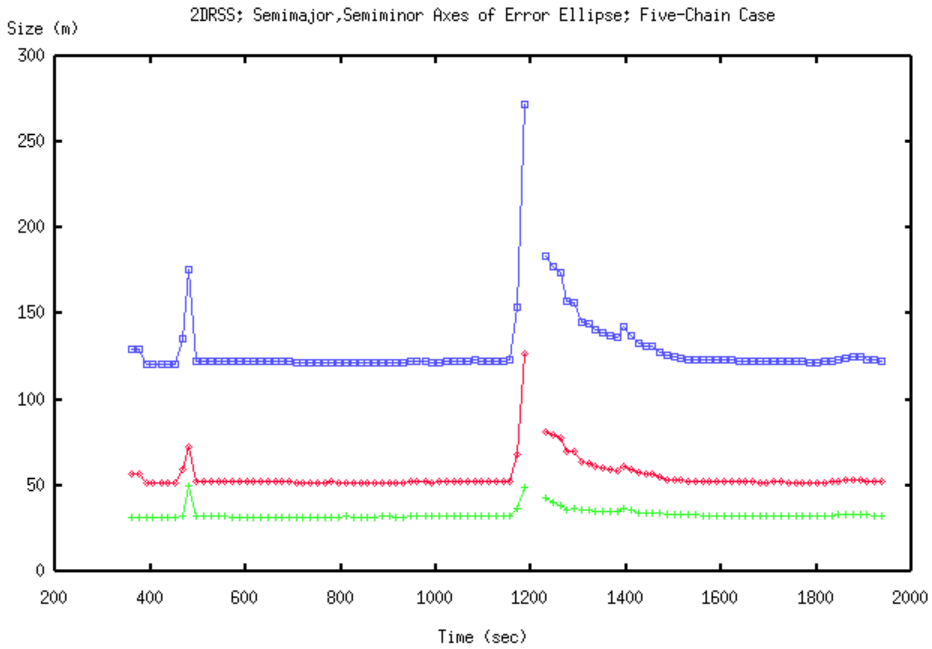


Figure 6. 2DRSS position error and lengths of the semimajor and semiminor axes of the error ellipse for the five-chain case after fault detection and exclusion via the t-test.

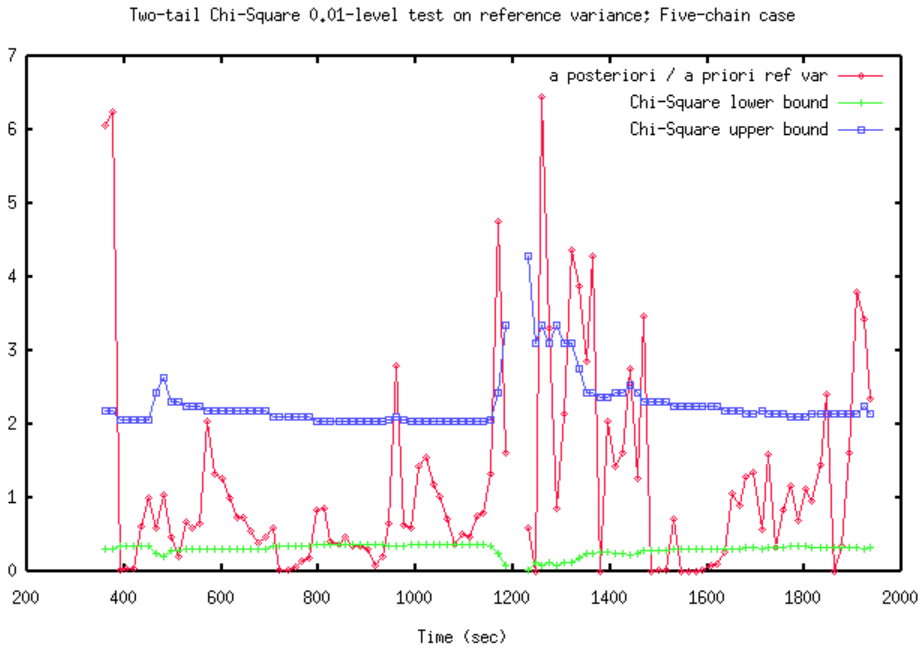


Figure 7. Chi-square testing of the a posteriori reference variance for the five-chain case. The bounds refer to the thresholds given in Table 1 divided by the degrees of freedom.

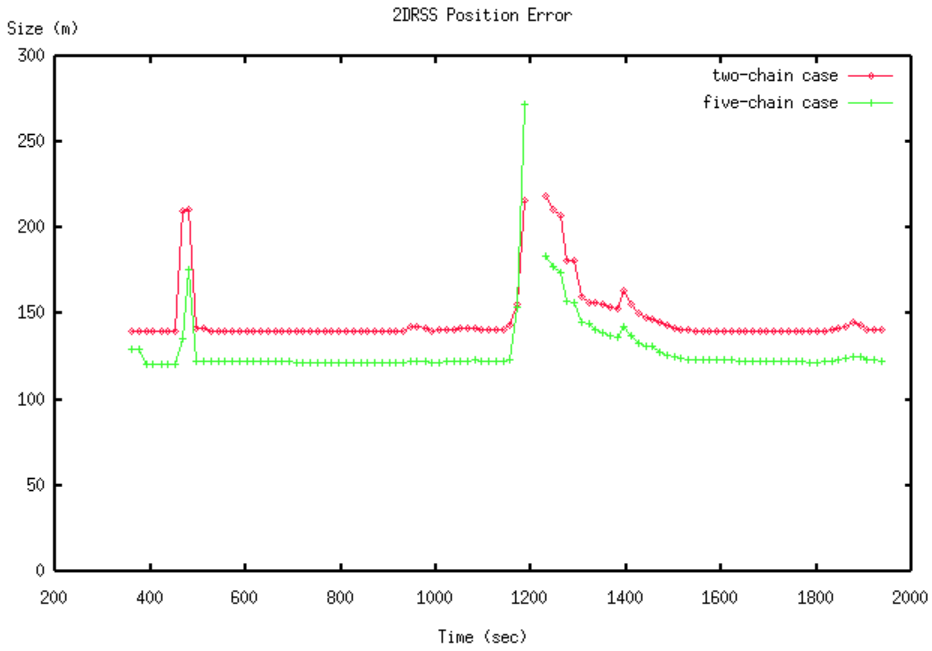


Figure 8. 2DRSS position error for the two-chain and five-chain cases.

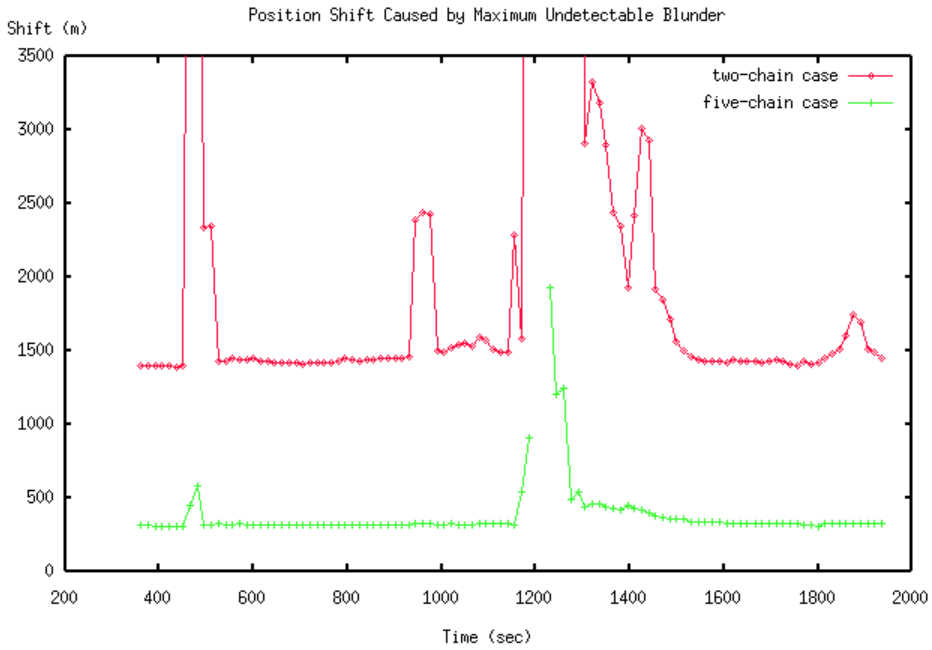


Figure 9. Position shift caused by the maximum undetectable blunder for the two-chain and five-chain cases.

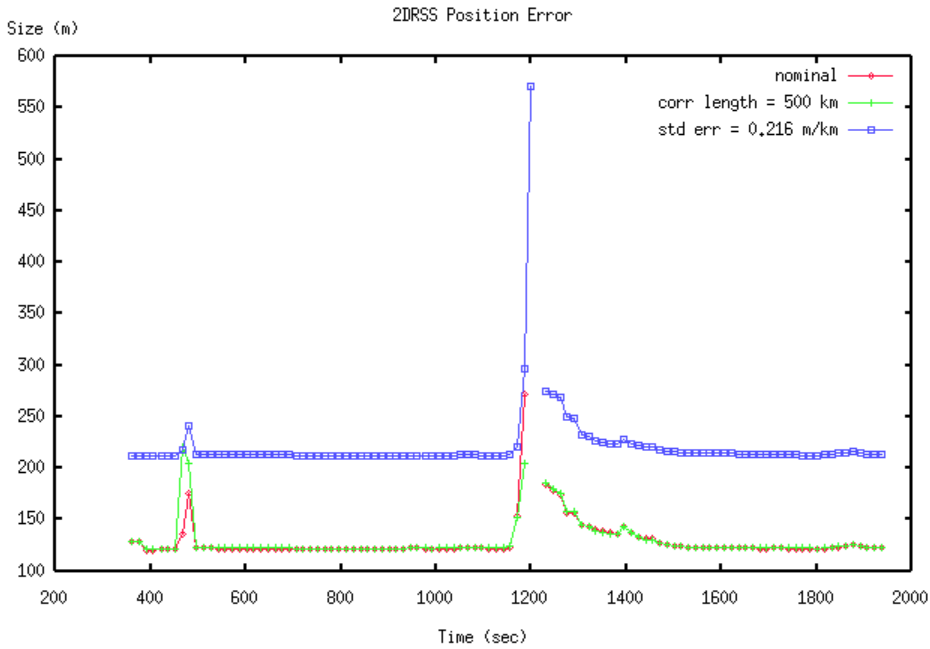


Figure 10. 2DRSS position error for the five-chain case and different assumptions about the scale factor error: (a) nominal, (b) correlation length increased from 200 to 500 km, and (c) standard error doubled to 0.216 m/km. The plots for cases (a) and (b) mostly overlap.

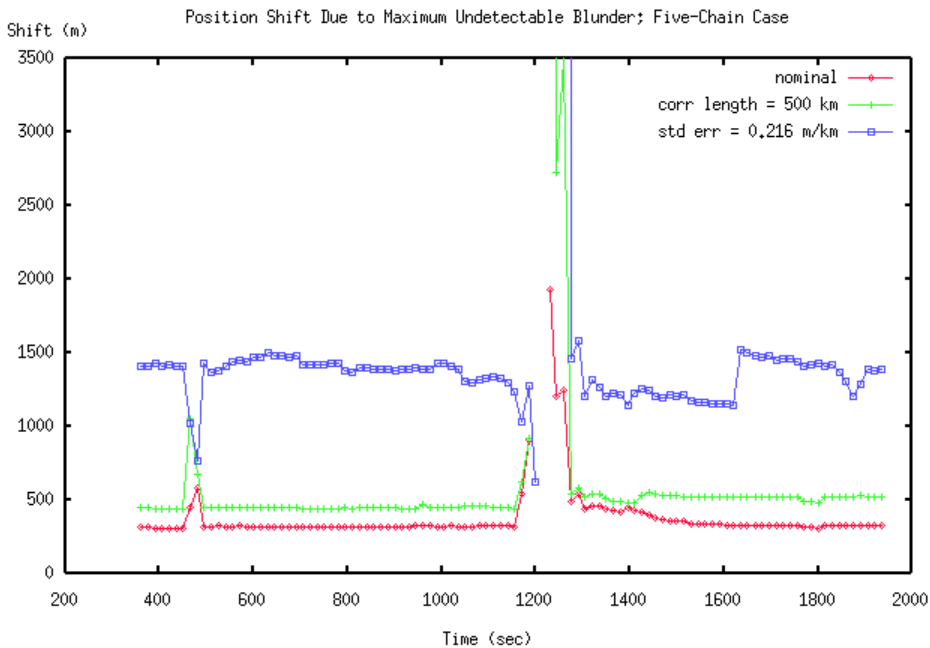


Figure 11. Position shift caused by the maximum undetectable blunder for the five-chain case and different assumptions about the scale factor error: (a) nominal, (b) correlation length increased from 200 to 500 km, and (c) standard error doubled to 0.216 m/km.